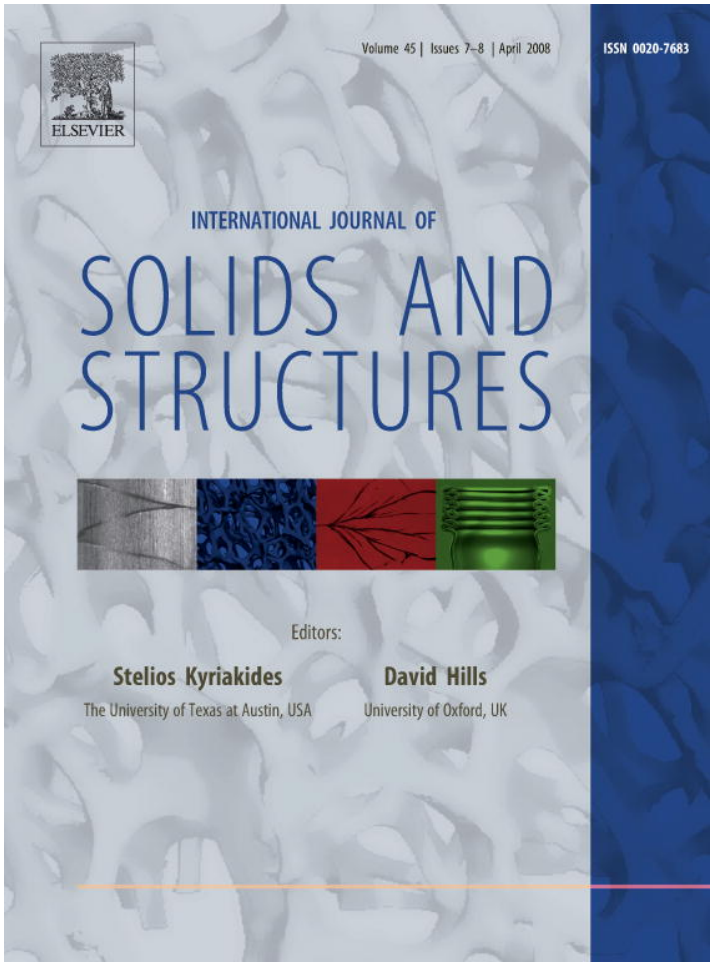

Available online at www.sciencedirect.com
ScienceDirect
International Journal of Solids and Structures 45 (2008) 2014–2023
INTERNATIONAL JOURNAL OF SOLIDS AND STRUCTURES
www.elsevier.com/locate/ijsolstr

Post-buckling analysis for the precisely controlled buckling of thin film encapsulated by elastomeric substrates

Hanqing Jiang [a,*], Yugang Sun [b], John A. Rogers [c,d], Yonggang Huang [e]

[a] Department of Mechanical and Aerospace Engineering, Arizona State University, Tempe, AZ 85287, USA
[b] Center for Nanoscale Materials, Argonne National Laboratory, 9700 South Cass Avenue, Argonne, IL 60439, USA
[c] Department of Materials Science and Engineering, Beckman Institute, and Seitz Materials Research Laboratory, University of Illinois at Urbana-Champaign, 1304 West Green Street, Urbana, IL 61801, USA
[d] Department of Mechanical Science and Engineering, University of Illinois at Urbana-Champaign, Urbana, IL 61801, USA
[e] Department of Civil and Environmental Engineering and Department of Mechanical Engineering, Northwestern University, Evanston, IL 60208, USA

Received 31 July 2007; received in revised form 10 November 2007
Available online 3 December 2007

Abstract

The precisely controlled buckling of stiff thin films (e.g., Si or GaAs nano ribbons) on the patterned surface of elastomeric substrate (e.g., poly(dimethylsiloxane) (PDMS)) with periodic inactivated and activated regions was designed by Sun et al. [Sun, Y., Choi, W.M., Jiang, H., Huang, Y.Y., Rogers, J.A., 2006. Controlled buckling of semiconductor nanoribbons for stretchable electronics. Nature Nanotechnology 1, 201–207] for important applications of stretchable electronics. We have developed a post-buckling model based on the energy method for the precisely controlled buckling to study the system stretchability. The results agree with Sun et al.'s (2006) experiments without any parameter fitting, and the system can reach 120% stretchability.

Keywords: Stretchable electronics; Buckling; Mechanics

1. Introduction

Buckling of a stiff thin film (e.g., silicon) on a compliant substrate [such as poly(dimethylsiloxane) (PDMS)], was first observed by Bowden et al. (1998), where the stiff thin films were attached on the unembellished surface of compliant substrate that is subject to pre-strain. Relaxation of the pre-strain in compliant substrate leads to buckling of stiff thin films with highly periodic, sinusoidal wavy patterns. The wavelength of the buckled film ranges from 10 to 100 μm. The buckling of stiff thin film/compliant substrate system has then been attracting lots of attentions due to its many important applications. For example, these applications include stretchable electronic interconnects (Lacour et al., 2004, 2005, 2003, 2006; Wagner et al., 2004), and stretch-

* Corresponding author.
E-mail address: hanqing.jiang@asu.edu (H. Jiang).

0020-7683/$ - see front matter © 2007 Elsevier Ltd. All rights reserved.
doi:10.1016/j.ijsolstr.2007.11.007

able electronic devices (Choi and Rogers, 2003; Choi et al., 2007; Jiang et al., 2007a,b; Khang et al., 2006), microelectromechanical systems (MEMS) and nanoelectromechanical systems (NEMS) (Fu et al., 2006), tunable phase optics (Efimenko et al., 2005; Harrison et al., 2004), force spectroscopy in cells (Harris et al., 1980), biocompatible topographic matrices for cell alignment (Teixeira et al., 2003), modern metrology methods (Stafford et al., 2005, 2004, 2006; Wilder et al., 2006), and other micro/nanofabrication (Bowden et al., 1999; Huck et al., 2000; Schmid et al., 2003; Sharp and Jones, 2002; Yoo et al., 2002).

The geometry of buckled thin film, however, is completely determined by the thin film thickness and the elastic moduli of the thin film and substrate, and therefore cannot be controlled once the thin film and substrate are specified. This "un-controlled" buckling may lead to some restrictions in applications. For stretchable electronics, the stretchable strain may reach 20% (Khang et al., 2006), which is much larger than the failure strain of silicon (~1%), but is still too small for certain applications. In order to control the buckle geometries and improve the stretchability, Sun et al. (2006) designed a mechanical strategy to fabricate precisely controlled buckle geometries for GaAs and Si nanoribbons on PMDS substrate, by using the photolithograph method to pattern PDMS surface and a buckling process similar to that reported in Khang et al. (2006).

We briefly summarized the fabrication procedure (Sun et al., 2006) in the following. Fig. 1a illustrates the photolithograph process that defines the bonding chemistry on a stretched PDMS substrate subject to pre-strain $\varepsilon_{pre} = \frac{\Delta L}{L}$ in the ribbon direction. The standard photolithograph method was used to form periodic interfacial patterns with activated sites where strong chemical bonds can form between PDMS substrate and thin

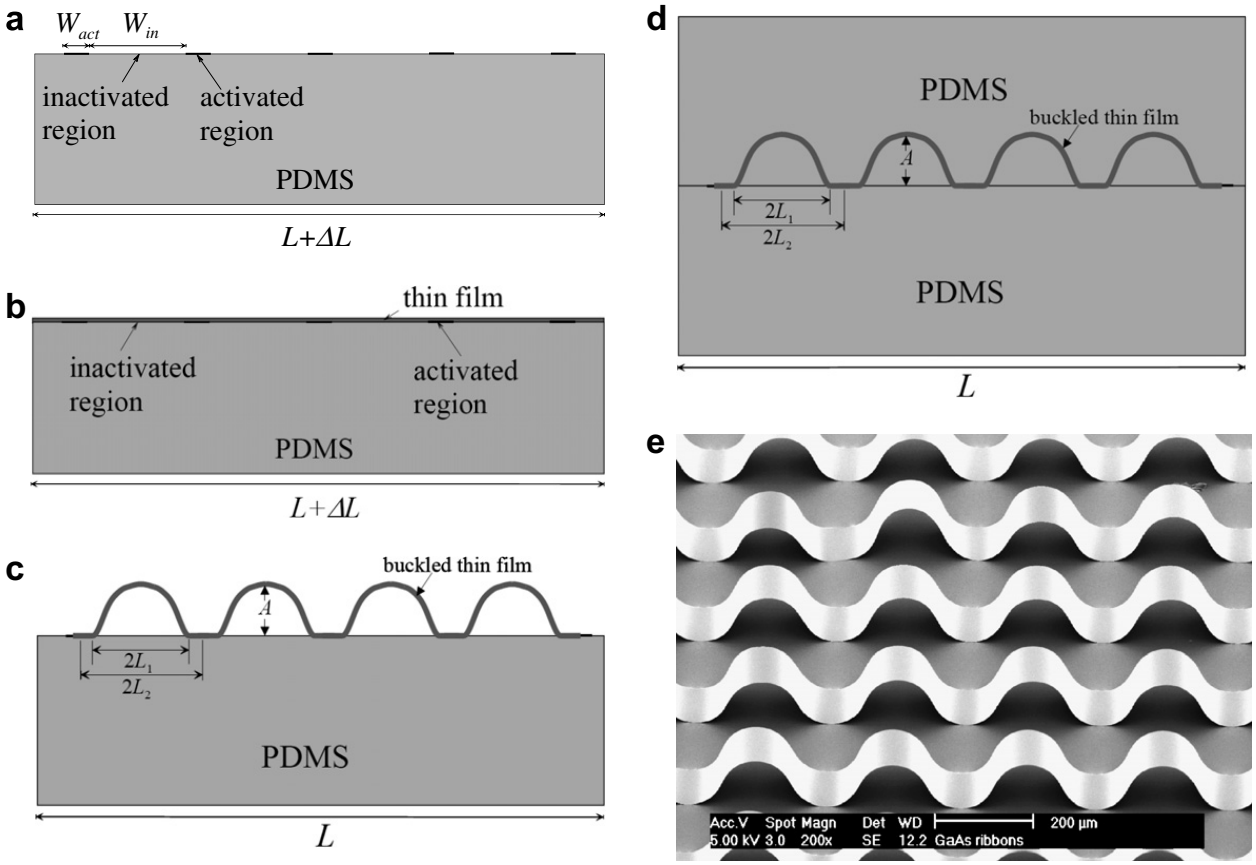

Fig. 1. Processing steps for precisely controlled thin film buckling on PDMS substrate. (a) Pre-strained PDMS with periodic activated and inactivated patterns. L is the original length of PDMS and ΔL is the extension. W_{act} and W_{in} denote the widths of activated and inactivated sites, respectively. (b) A thin film parallel to the pre-strain direction is attached to the pre-strained and patterned PDMS substrate. (c) The relaxation of the pre-strain ε_{pre} in PDMS leads to buckles of thin film. The wavelength of the buckled film is $2L_1$, and its amplitude is A. $2L_2$ is the sum of activated and inactivated regions after relaxation. (d) Casting and curing a liquid prepolymer to encapsulate the buckled nanoribbons into PDMS substrates. (e) Scanning electron microscope (SEM) image of buckled GaAs thin films formed using the previous procedures.

films (GaAs or Si), as well as inactivated sites where there only exist weak van der Waals interactions at the interface. Let W_{act} and W_{in} denote the widths of activated and inactivated sites, respectively (Fig. 1a). Fig. 1b shows the second step where the thin film ribbons are aligned parallel to the pre-strain direction on the pre-strained and patterned PDMS substrate, followed by the third step (Fig. 1c) where the relaxation of the pre-strain ε_{pre} in PDMS leads to the buckled thin film ribbons due to the physical separation from the inactivated sites. The strong chemical bonding over the activated region keeps the ribbons on PDMS. The wavelength of the buckled structures is $2L_1 = \frac{W_{in}}{1+\varepsilon_{pre}}$, which is well controlled by the interfacial patterns (W_{in}). The amplitude A of the buckled thin films also depends on the geometries of the interfacial patterns (W_{act} and W_{in}) and the pre-strain, and is to be determined. Finally, the buckled thin films are encapsulated in PDMS (i.e., buckled thin film is sandwiched by PDMS) by casting and curing a liquid prepolymer that can flow and fill the gaps between buckled thin films and PDMS substrates (Fig. 1d). Fig. 1e shows the scanning electron microscope (SEM) image of buckled GaAs thin films formed using this method.

Jiang et al. (2007a,b) developed a nonlinear buckling model to analyze the initial-buckling (Fig. 1a–c), and obtained the simple analytical expressions for the wavelength and amplitude of initial buckled geometry, as well as the maximum strain in the thin film. For stretchable electronics, it is important to study the post-buckling behavior and answer the following two questions:

(1) How does the buckled thin film deform when subject to external strains?
(2) What is the theoretically achievable stretchability for such controlled buckling thin films sandwiched by two pieces of PDMS shown in Fig. 1d?

These two questions are answered in this paper based on a post-buckling analysis for the buckled system shown in Fig. 1d. The initial-buckling analysis (Jiang et al., 2007a,b) is firstly reviewed to pave the way for the post-buckling analysis.

2. Initial-buckling model: a brief review

The initial-buckling analysis (Jiang et al., 2007b) is briefly summarized in this section. It is based on the energy method, which has also been used in other studies of buckled stiff thin film/compliant substrate systems (e.g., Huang et al., 2005). The total energy U_{tot} in the thin film/substrate system consists of three parts, the bending energy U_b due to thin film buckling, membrane energy U_m in the thin film, and substrate energy U_s. The bending and membrane energies of the thin film are given by

$$U_b = \int_{-L_2}^{L_2} \frac{1}{2} \frac{h^3 \overline{E}_f}{12} \left(\frac{d^2 w}{dx_1^2} \right)^2 dx_1, \tag{1}$$

$$U_m = \int_{-L_2}^{L_2} \frac{1}{2} h \overline{E}_f \varepsilon_{11}^2 \, dx_1, \tag{2}$$

where h is the film thickness, the plane-strain modulus $\overline{E}_f = E_f/(1-\nu_f^2)$ is related to the Young's modulus E_f and Poisson's ratio ν_f of the thin film, x_1 is the ribbon direction, w is the buckling profile (deflection), ε_{11} is the membrane strain, $2L_1 = \frac{W_{in}}{1+\varepsilon_{pre}}$ is the initial-buckling wavelength; and $2L_2 = 2L_1 + W_{act}$ is the sum of activated and inactivated regions after relaxation (Fig. 1c), respectively. Based on Fig. 1c, the buckling profile can be expressed as

$$w = \begin{cases} w_1^0 = \frac{1}{2} A \left(1 + \cos \frac{\pi x_1}{L_1} \right), & -L_1 < x_1 < L_1 \\ w_2^0 = 0, & L_1 < |x_1| < L_2 \end{cases}, \tag{3}$$

where the subscript "0" denotes the initial-buckling, and the buckling amplitude A is to be determined. The bending energy U_b is then obtained from Eq. (1).

The membrane strain ε_{11} is related to the deflection w in Eq. (3) and the in-plane displacement u_1 via von Karman beam theory (Timoshenko and Gere, 1961)

$$\varepsilon_{11} = \frac{\mathrm{d}u_1}{\mathrm{d}x_1} + \frac{1}{2}\left(\frac{\mathrm{d}w}{\mathrm{d}x_1}\right)^2 - \varepsilon_{\mathrm{pre}}, \tag{4}$$

where the relaxation of pre-strain $\varepsilon_{\mathrm{pre}}$ in the substrate causes a compressive strain $-\varepsilon_{\mathrm{pre}}$ in the thin film. The in-plane displacement u_1 is determined from the force equilibrium of the thin film with vanishing shear at the interface (Huang et al., 2005), which gives a constant membrane strain $\varepsilon_{11} = \frac{A^2\pi^2}{16L_1L_2} - \varepsilon_{\mathrm{pre}}$. The membrane energy in the thin film is then obtained from Eq. (2).

Once the pre-strain in the substrate is relaxed, the substrate deformation results completely from the displacement/stress traction at the film/substrate interface. The stress traction is zero over the buckled regions of the thin film, i.e., the inactivated regions ($2L_1$). For activated regions, Sun et al. (2006) observed in the scanning electron microscope (SEM) that the thin film/substrate interface [$W_{\mathrm{act}} = 2(L_2 - L_1)$] remains flat and exerts vanishing displacement to the substrate. For vanishing displacement and vanishing stress traction, the relaxed substrate has vanishing energy, $U_{\mathrm{s}} = 0$.

Minimization of total energy $\frac{\partial U_{\mathrm{tot}}}{\partial A} = 0$ with respect to the buckling amplitude A gives

$$A = \begin{cases} \frac{2}{\pi(1+\varepsilon_{\mathrm{pre}})}\sqrt{W_{\mathrm{in}}[W_{\mathrm{in}} + W_{\mathrm{act}}(1+\varepsilon_{\mathrm{pre}})](\varepsilon_{\mathrm{pre}} - \varepsilon_{\mathrm{c}})}, & \text{for } \varepsilon_{\mathrm{pre}} \geqslant \varepsilon_{\mathrm{c}} \\ 0 & \text{for } \varepsilon_{\mathrm{pre}} < \varepsilon_{\mathrm{c}} \end{cases}, \tag{5}$$

where

$$\varepsilon_{\mathrm{c}} = \frac{h^2\pi^2}{12L_1^2} \tag{6}$$

is the critical strain for initial buckling, which is on the order of 10^{-6} for the buckling wavelength $2L_1 \sim 200$ μm and thin film thickness $h \sim 0.1$ μm.

The constant membrane strain $\varepsilon_{11} = \frac{A^2\pi^2}{16L_1L_2} - \varepsilon_{\mathrm{pre}}$ is very small ($\sim 10^{-6}$). Therefore the maximum strain in the thin film is the bending strain due to the thin film curvature $\frac{\mathrm{d}^2w}{\mathrm{d}x_1^2}$, i.e.,

$$\varepsilon_{\max} = \frac{h}{2}\max\left(\frac{\mathrm{d}^2w}{\mathrm{d}x_1^2}\right) = \frac{2h\pi(1+\varepsilon_{\mathrm{pre}})}{W_{\mathrm{in}}}\sqrt{\left[1 + \frac{W_{\mathrm{act}}}{W_{\mathrm{in}}}(1+\varepsilon_{\mathrm{pre}})\right]\varepsilon_{\mathrm{pre}}}. \tag{7}$$

Since the activated region W_{act} and the thin film thickness h (~ 0.1 μm) are much smaller than the inactivated region W_{in}, the maximum strain $\varepsilon_{\max}$ is much smaller than pre-strain $\varepsilon_{\mathrm{pre}}$. For a 0.3 μm thin GaAs film buckled on a patterned PDMS substrate with $W_{\mathrm{act}} = 10$ μm, $W_{\mathrm{in}} = 400$ μm and $\varepsilon_{\mathrm{pre}} = 60\%$, the maximum strain in the thin film is only 0.6%, two orders of magnitude smaller than the 60% prestrain.

3. Post-buckling analysis

The buckled thin films are protected by casting and curing of a prepolymer (Fig. 1d), which is fluid that can flow and fill the air gaps between buckled thin film and PDMS substrate (Sun et al., 2006). Once the liquid prepolymer is cured and solidified, the buckled thin films are then encapsulated between PDMS substrates (Fig. 1d), and are ready to be subject to the externally applied strain $\varepsilon_{\mathrm{applied}}$. Such a sandwiching procedure does not change the wavelength ($2L_1$) or the amplitude (A) of the buckled thin film because the prepolymer is liquid and does not impose any deformation to the thin film. A post-buckling model is developed in this section to study how the amplitude and wavelength change to accommodate the applied strain and predict the theoretically achievable stretchability.

3.1. Post-buckling profile and bending energy in the thin film

Upon the applied strain $\varepsilon_{\mathrm{applied}}$ the initial-buckling geometry given in Eq. (3) changes to

$$w=\begin{cases} w_1=w_1^0+w_1^{\mathrm{c}}=\frac{1}{2}A\left(1+\cos\frac{\pi x_1}{L_1}\right)+A_1^{\mathrm{c}}\cos k_1x_1, & -L_1<x_1<L_1 \\ w_2=w_2^0+w_2^{\mathrm{c}}=A_2^{\mathrm{c}}\cos(k_2x_1+\phi_2)+C_2, & L_1<|x_1|<L_2 \end{cases}, \tag{8}$$

where $w_1^{\mathrm{c}}=A_1^{\mathrm{c}}\cos k_1x_1$ and $w_2^{\mathrm{c}}=A_2^{\mathrm{c}}\cos(k_2x_1+\phi_2)+C_2$ are the changes of the deflection due to $\varepsilon_{\mathrm{applied}}$, which involves six parameters $(A_1^{\mathrm{c}},\ A_2^{\mathrm{c}},\ k_1,\ k_2,\ \phi_2,\ C_2)$ to be determined.

There are four continuity conditions across the interface between inactivated and activated regions ($x_1=\pm L_1$), i.e., the continuity of deflection ($w_1^{\mathrm{c}}|_{x_1=\pm L_1}=w_2^{\mathrm{c}}|_{x_1=\pm L_1}$), rotation $\left(\left.\frac{\mathrm{d}w_1^{\mathrm{c}}}{\mathrm{d}x_1}\right|_{x_1=\pm L_1}=\left.\frac{\mathrm{d}w_2^{\mathrm{c}}}{\mathrm{d}x_1}\right|_{x_1=\pm L_1}\right)$, bending moment $\left(\left.\frac{\mathrm{d}^2w_1^{\mathrm{c}}}{\mathrm{d}x_1^2}\right|_{x_1=\pm L_1}=\left.\frac{\mathrm{d}^2w_2^{\mathrm{c}}}{\mathrm{d}x_1^2}\right|_{x_1=\pm L_1}\right)$, and shear force $\left(\left.\frac{\mathrm{d}^3w_1^{\mathrm{c}}}{\mathrm{d}x_1^3}\right|_{x_1=\pm L_1}=\left.\frac{\mathrm{d}^3w_2^{\mathrm{c}}}{\mathrm{d}x_1^3}\right|_{x_1=\pm L_1}\right)$. The periodic condition of the entire activated/inactivated regions requires $\frac{\mathrm{d}w_2^{\mathrm{c}}}{\mathrm{d}x_1}=0$ at $x_1=\pm L_2$. These five conditions relate the six parameters $(A_1^{\mathrm{c}},\ A_2^{\mathrm{c}},\ k_1,\ k_2,\ \phi_2,\ C_2)$ to one (e.g., A_1^{c}), and yield two sets of solutions. The first corresponds to $A_2^{\mathrm{c}}=A_1^{\mathrm{c}},\ k_1=k_2=\frac{n\pi}{L_2},\ \phi_2=0$ and $C_2=0$, and is called the unified post-buckling mode since the activated and inactivated regions have a unified expression

$$w_1^{\mathrm{c}}=w_2^{\mathrm{c}}=A_1^{\mathrm{c}}\cos\frac{n\pi x_1}{L_2}, \tag{9}$$

where n is an integer. The second solution gives $A_2^{\mathrm{c}}=\left[\frac{n(L_2-L_1)}{(m-n)L_1}\right]^2A_1^{\mathrm{c}},\ k_1=\frac{n\pi}{L_1},\ k_2=\frac{(m-n)\pi}{L_2-L_1},\ \phi_2=\frac{(nL_2-mL_1)\pi}{L_2-L_1}$ and $C_2=(-1)^n(A_1^{\mathrm{c}}-A_2^{\mathrm{c}})$, which is called the non-unified post-buckling mode,

$$w_1^{\mathrm{c}}=A_1^{\mathrm{c}}\cos\frac{n\pi x_1}{L_1} \tag{10}$$

for the inactivated region and

$$w_2^{\mathrm{c}}=A_1^{\mathrm{c}}\left[\frac{n(L_2-L_1)}{(m-n)L_1}\right]^2\left\{\cos\left[\frac{m(x_1-L_1)+n(L_2-x_1)}{L_2-L_1}\pi\right]+(-1)^{n-1}\right\}+(-1)^nA_1^{\mathrm{c}} \tag{11}$$

for the activated region, which can be equivalently expressed as

$$w_2^{\mathrm{c}}=(-1)^nA_1^{\mathrm{c}}\left[\frac{nW_{\mathrm{act}}}{2(m-n)L_1}\right]^2\left\{\cos\left[\frac{2(m-n)(x_1-L_1)}{W_{\mathrm{act}}}\pi\right]-1\right\}+(-1)^nA_1^{\mathrm{c}},$$

where n and m are two integers. For this non-unified post-buckling mode, the rotation vanishes at the interface between the activated and inactivated regions, $\left.\frac{\mathrm{d}w_1^{\mathrm{c}}}{\mathrm{d}x_1}\right|_{x_1=\pm L_1}=\left.\frac{\mathrm{d}w_2^{\mathrm{c}}}{\mathrm{d}x_1}\right|_{x_1=\pm L_1}=0$.

The bending energy can be obtained by

$$U_{\mathrm{b}}=2\int_{L_1}^{L_2}\frac{1}{2}\frac{\overline{E}_{\mathrm{f}}h^3}{12}\left(\frac{\mathrm{d}^2w_2}{\mathrm{d}x_1^2}\right)^2\mathrm{d}x_1+\int_{-L_1}^{L_1}\frac{1}{2}\frac{\overline{E}_{\mathrm{f}}h^3}{12}\left(\frac{\mathrm{d}^2w_1}{\mathrm{d}x_1^2}\right)^2\mathrm{d}x_1. \tag{12}$$

For the unified post-buckling mode (Eq. (9)), the bending energy is

$$U_{\mathrm{b}}=\frac{\overline{E}_{\mathrm{f}}h^3}{24}\left[\frac{A^2\pi^4+4(A_1^{\mathrm{c}})^2k_1^4L_1^3L_2}{4L_1^3}-\frac{2AA_1^{\mathrm{c}}\pi^2k_1^3\sin(k_1L_1)}{(k_1L_1)^2-\pi^2}\right]. \tag{13}$$

For the non-unified post-buckling mode (Eqs. (10) and (11)), the bending energy is

$$U_{\mathrm{b}}=\frac{\overline{E}_{\mathrm{f}}h^3}{24}\left[\frac{A^2\pi^4+4(A_1^{\mathrm{c}})^2k_1^4L_1^4+4(A_2^{\mathrm{c}})^2k_2^4L_1^3(L_2-L_1)}{4L_1^3}\right]. \tag{14}$$

3.2. Membrane energy for the thin film

The force equilibrium of the thin film requires (Huang et al., 2005; Timoshenko and Gere, 1961)

$$\frac{\partial N_{11}}{\partial x_1} = T_1, \tag{15}$$

where $N_{11} = h\overline{E}_f\varepsilon_{11}$ is the membrane force and T_1 is the shear stress at the thin film/substrate interface. Huang et al. (2005) showed that the shear stress at the interface between a stiff thin film and a compliant substrate is negligible, which implies constant membrane force N_{11} and constant membrane strain ε_{11} given by

$$\varepsilon_{11} = \frac{\mathrm{d}u_1}{\mathrm{d}x_1} + \frac{1}{2}\left(\frac{\mathrm{d}w}{\mathrm{d}x_1}\right)^2 - \varepsilon_{\mathrm{pre}} + \varepsilon_{\mathrm{applied}} \tag{16}$$

due to applied strain $\varepsilon_{\mathrm{applied}}$. The in-plane displacement u_1 also satisfies

$$\int_{-L_2}^{L_2} \frac{\mathrm{d}u_1}{\mathrm{d}x_1}\,\mathrm{d}x_1 = 0. \tag{17}$$

to be consistent with the overall substrate deformation (Chen and Hutchinson, 2004). This gives the membrane strain

$$\varepsilon_{11} = \frac{A^2\pi^2 + 4(A_1^c k_1)^2 L_1 L_2}{16 L_1 L_2} + \frac{A A_1^c k_1 \pi^2 \sin(k_1 L_1)}{2L_2[\pi^2 - (L_1 k_1)^2]} - \varepsilon_{\mathrm{pre}} + \varepsilon_{\mathrm{applied}} \tag{18}$$

for unified post-buckling mode Eq. (9) and

$$\varepsilon_{11} = \frac{A^2\pi^2 + 4(A_1^c k_1 L_1)^2 + 4(A_2^c k_2)^2 L_1(L_2 - L_1)}{16 L_1 L_2} - \varepsilon_{\mathrm{pre}} + \varepsilon_{\mathrm{applied}} \tag{19}$$

for the non-unified post-buckling model (Eqs. (10) and (11)). The membrane energy is given by

$$U_m = \int_{-L_2}^{L_2} \tfrac{1}{2} h\overline{E}_f \varepsilon_{11}^2\,\mathrm{d}x_1 = h\overline{E}_f L_2 \varepsilon_{11}^2. \tag{20}$$

3.3. Substrate energy

As discussed in Section 2, the embedding procedure does not induce any deformation such that the relaxed substrates are strain free. For post-buckling, the substrate energy results solely from the changes of deflection, either for the unified post-buckling mode (Eq. (9)) or for the non-unified post-buckling mode (Eqs. (10) and (11)).

Each substrate is subject to the applied strain $\varepsilon_{\mathrm{applied}}$ in ribbon direction (x_1), and is modeled as a two-dimensional semi-infinite elastic solid since the substrate thickness is several orders of magnitude larger than the thin film thickness. The strain energy for both substrates is obtained via the divergence theorem as

$$U_s = \int_{-L_2}^{L_2} T_3 w^c\,\mathrm{d}x_1, \tag{21}$$

where the periodic conditions at $x_1 = \pm L_2$ have been used, T_3 is the normal traction resulting from the post-buckling mode w^c in Eq. (9) or (10) and (11) at the film/substrate interface ($x_3 = 0$).

(1) *Unified post-buckling mode*

The normal traction for the unified post-buckling mode (Eq. (9)) is

$$T_3 = \frac{1}{2}\overline{E}_s k_1 A_1^c \cos(k_1 x_1), \tag{22}$$

where $\overline{E}_s = E_s/(1 - \nu_s^2)$ is the plane-strain modulus of the substrate. The strain energy in the substrates is

$$U_s = \frac{1}{2}\overline{E}_s (A_1^c)^2 k_1 L_2. \tag{23}$$

(2) *Non-unified post-buckling mode*

The post-buckling mode in Eqs. (10) and (11) is periodic over $[-L_2, L_2]$, and can be expressed in the Fourier series as

$$w_{\mathrm{F}} = \frac{1}{2}a_0 + \sum_{i=1}^{\infty} a_i \cos\left(\frac{i\pi x_1}{L_2}\right), \tag{24}$$

where $a_i = \frac{2}{L_2}\int_0^{L_2} w^{\mathrm{c}} \cos\left(\frac{i\pi x_1}{L_2}\right) \mathrm{d}x_1$ $(i = 0, 1, 2, \ldots)$ are linearly proportional to A_1^{c}. Each term $a_i \cos\left(\frac{i\pi x_1}{L_2}\right)$ in the Fourier series mimics a unified post-buckling mode, and corresponds to the normal traction $T_3^i = \frac{ia_i\pi}{2L_2}\overline{E}_{\mathrm{s}} \cos\left(\frac{i\pi x_1}{L_2}\right)$ at the film/substrate interface. This gives the total normal traction

$$T_3 = \sum_{i=1}^{\infty} T_3^i = \frac{\pi}{2L_2}\overline{E}_{\mathrm{s}} \sum_{i=1}^{\infty} i a_i \cos\left(\frac{i\pi x_1}{L_2}\right), \tag{25}$$

and the strain energy in the substrates

$$U_{\mathrm{s}} = \int_{-L_2}^{L_2} T_3 w_{\mathrm{F}} \,\mathrm{d}x_1 = \frac{\pi}{2}\overline{E}_{\mathrm{s}} \sum_{i=1}^{\infty} i a_i^2, \tag{26}$$

where w_{F} is the deflection expressed in the Fourier series given by Eq. (24).

3.4. Energy minimization

The total strain energy in the system is the summation of membrane and bending energy in the thin film and the strain energy in the substrate, $U_{\mathrm{tot}} = U_{\mathrm{m}} + U_{\mathrm{b}} + U_{\mathrm{s}}$. It depends on a single variable, A_1^{c}, which is determined analytically by energy minimization, i.e., $\partial U_{\mathrm{tot}}/\partial A_1^{\mathrm{c}} = 0$, for both unified post-buckling mode (Eq. (9)) and non-unified post-buckling mode (Eqs. (10) and (11)). For unified post-buckling mode, the energy minimization gives a cubic equation

$$\alpha_3 \left(A_1^{\mathrm{c}}\right)^3 + \alpha_2 \left(A_1^{\mathrm{c}}\right)^2 + \alpha_1 A_1^{\mathrm{c}} + \alpha_0 = 0, \tag{27}$$

where

$$\alpha_3 = k_1^3,$$

$$\alpha_2 = \frac{3A\pi^2 k_1^2 \sin(k_1 L_1)}{L_2[\pi^2 - (k_1 L_1)^2]},$$

$$\alpha_1 = \frac{2A^2\pi^4 k_1 \sin^2(k_1 L_1)}{L_2^2[\pi^2 - (k_1 L_1)^2]^2} + 4\left(\frac{A^2\pi^2}{16L_1 L_2} + \varepsilon_{\mathrm{applied}} - \varepsilon_{\mathrm{pre}}\right)k_1 + \frac{1}{3}h^2 k_1^3 + 4\frac{\overline{E}_{\mathrm{s}}}{h\overline{E}_{\mathrm{f}}},$$

$$\alpha_0 = \frac{A\pi^2 \sin(k_1 L_1)}{L_2[\pi^2 - (k_1 L_1)^2]}\left[4\left(\frac{A^2\pi^2}{16L_1 L_2} + \varepsilon_{\mathrm{applied}} - \varepsilon_{\mathrm{pre}}\right) + \frac{k_1^2 h^2}{3}\right].$$

The numerical method is then used to solve this cubic equation. The similar cubic equation for the non-unified post-buckling mode can be correspondingly obtained.

For unified buckling mode (Eq. (9)), the total potential energy is evaluated for n ranging from 1 to 100. For non-unified buckling mode (Eq. (10)), sufficient terms in the Fourier series are taken to ensure the convergence, and without losing generality, the total potential energy is evaluated for $m > n$. The total potential energies for these two buckling modes are compared to determine the energetically favorable one. As shown in Section 4, both buckling models will occur depending on the external strain $\varepsilon_{\mathrm{applied}}$.

4. Results and discussion

We take GaAs nanoribbons and PDMS substrates as an example. The thickness of GaAs nanoribbons is 0.27 μm. The Young's modulus E_{f} and Poisson's ratio ν_{f} of GaAs are 85.5 GPa and 0.31, respectively. Its frac-

ture strain is about 2% (Sun et al., 2006). The Young's modulus of the PDMS substrate is $E_s = 2$ MPa, which is nearly five orders of magnitude more compliant than the thin film. The Poisson's ratio of the PDMS substrate is $\nu_s = 0.48$.

In order to compare with experiments (Sun et al., 2006), we study three patterned surfaces. They have the same length $W_{act} = 10$ μm for the activated region, but different lengths for the inactivated region. They are all subject to the same pre-strain, 60%. The first pattern has the length $W_{in} = 400$ μm for the inactivated region. The initial-buckling amplitude $A = 125.7$ μm is obtained from Eq. (5), and the initial-buckling profile is shown in Fig. 2a. The post-buckling profile is determined via the analysis in Section 3. The membrane strain ε_{11} (Eq. (16)) in both the activated and inactivated regions remains very small (on the order of 10^{-3}) during post-buckling, which suggests that the thin film strain is dominated by the bending strain.

Before the applied compressive strain reaches a critical value, which is $\varepsilon_{applied} = -24.7\%$ for the GaA thin film and PDMS substrates, the unified post-buckling mode (Eq. (9)) occurs. The corresponding mode number is $n = 1$ such that there is only a single wave over both inactivated and activated regions, as shown in Fig. 2b for $\varepsilon_{applied} = -15\%$. The amplitude and wavelength of this single wave vary to accommodate the applied strain. The bending strain (and therefore the thin film strain) increases with the applied strain, and is on the order of 1% for $\varepsilon_{applied} = -20\%$.

Once the applied compressive strain reaches the critical strain $\varepsilon_{applied} = -24.7\%$, the non-unified post-buckling mode in Eqs. (10) and (11) occurs, but the buckling mode number n is always larger than 1. Fig. 2c shows the post-buckling profile for $\varepsilon_{applied} = -24.7\%$. "Small" waves with wavelength on the order of 30 μm are observed, corresponding to $n = 6$ and $m = 7$ in the non-unified post-buckling mode. The bending strain increases sharply from less than 1% to more than 2% as soon as the non-unified post-buckling comes into play because of the large curvature induced by "small" waves, and may lead to the fracture of nanoribbons. Sun et al. (2006) observed those "small" waves in the experiments when the compressive strain reached -20.6%. Similar to Khang et al. (2006), the mechanism for the small waves is that "small" waves may relax the compressive strain in the thin film and reduce the membrane energy. The difference between the critical strains in

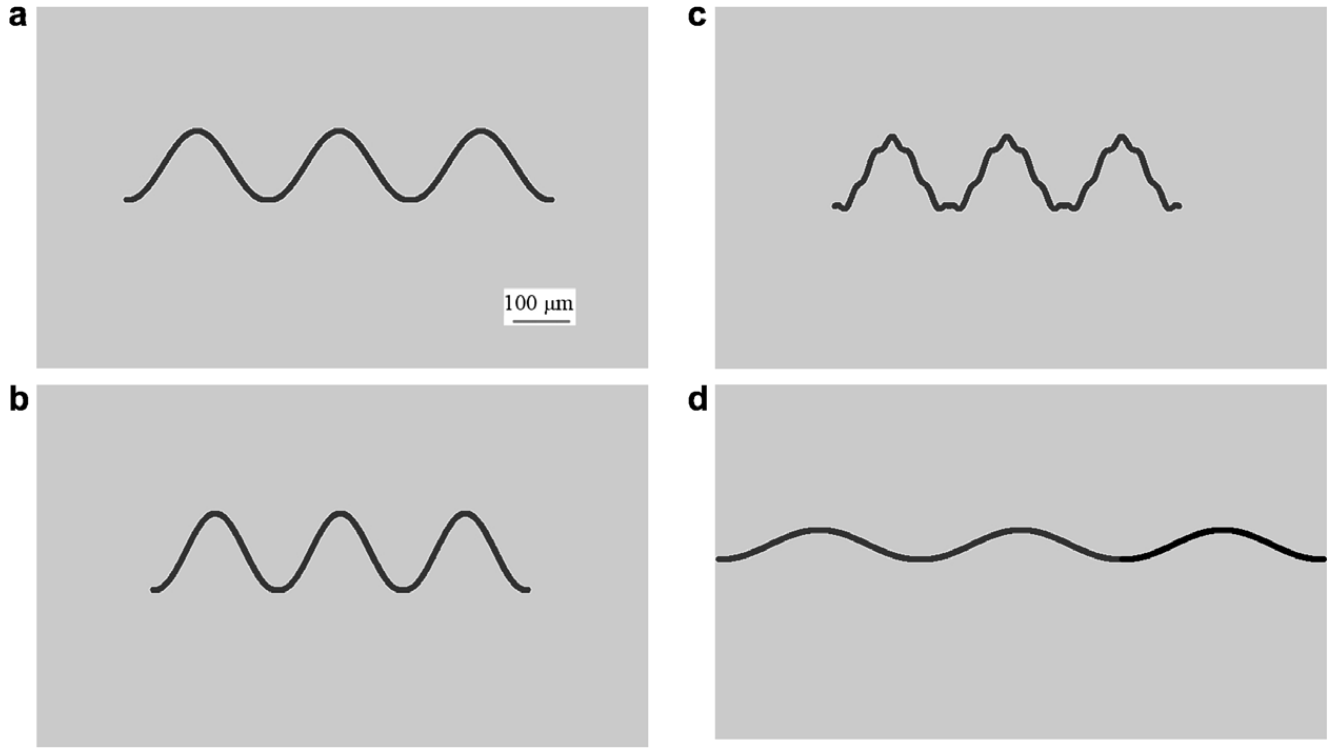

Fig. 2. Snap shots of buckling profile for different applied strain for given patterned surface ($W_{act} = 10$ μm, $W_{in} = 400$ μm) and 60% pre-strain. (a) Initial-buckling ($\varepsilon_{applied} = 0$) profile; (b) buckling profile at $\varepsilon_{applied} = -15\%$; (c) buckling profile at the critical point $\varepsilon_{applied} = -24.7\%$ at which the "small" waves appear and the nanoribbons break; and (d) buckling profile at $\varepsilon_{applied} = 50\%$.

our post-buckling analysis (−24.7%) and experiments (−20.6%) is partially because the peak of initial-buckling profile is flattened during sandwich procedure, which makes it easier to generate the "small" waves in experiments.

For the tensile applied strain ($\varepsilon_{applied} > 0$), the amplitude decreases and the wavelength increases. Only the unified post-buckling mode occurs, and there are no "small" waves. Fig. 2d shows a post-buckling profile with $\varepsilon_{applied} = 50\%$. As the tensile applied strain increases, the bending strain decreases and eventually the strain in the thin film becomes dominated by the membrane strain. For the tensile applied strain $\varepsilon_{applied} = 55.8\%$, the membrane strain reaches the fracture strain (2%) of GaA thin film, which agrees with the experiments (Sun et al., 2007). The post-buckling analysis shows that this patterned surface ($W_{act} = 10$ μm, $W_{in} = 400$ μm) can be stretched up to 55% and compressed up to 24%, i.e., about a total stretchability of 80%.

The other two patterned surfaces have shorter length for the inactivated region, $W_{in} = 300$ and 200 μm, respectively. For $W_{in} = 300$ μm, "small" waves appear and the thin film fracture when the compressive applied strain reaches −34.4%. The tensile stretchability is 57.6%, which agrees with Sun et al.'s (2006) experiments. The total stretchability is more than 90%. For $W_{in} = 200$ μm, "small" waves appear and the thin film fracture when the compressive applied strain reaches −57.1%. The tensile stretchability is 59.2%. This suggests that the decrease of the inactivated region (but still much longer than activated region) may increase the stretchability.

5. Conclusion remarks

We have developed a post-buckling model for the precisely controlled buckling of stiff thin films (e.g., GaAs) on the patterned surface of an elastomeric substrate (e.g., PDMS) with periodic inactivated and activated regions. The model, which is an extension of our prior initial-buckling analysis (Jiang et al., 2007b), gives the amplitude and wavelength of post-buckled profile. It also predicts that some "small" waves appear once the applied compressive strain reaches a critical value, and triggers the fracture of thin films. This agrees with Sun et al.'s (2006) experiments. The system of stiff thin films/compliant substrate, which has important applications in stretchable electronics, can reach the stretchability of 120%.

Acknowledgement

H.J. acknowledges the support from NSF CMMI-0700440. Y.S. acknowledges the support of the US Department of Energy, Office of Science, Office of Basic Energy Sciences, under contract DE-AC02-06CH11357. This work was also supported by the Defense Advanced Research Projects Agency – funded Air Force Research Laboratory – managed Macroelectronics Program Contract FA8650-04-C-7101, by the US Department of Energy under Grant DEFG02-91-ER45439, and by NSF under Grant DMI-0328162.

References

Bowden, N., Brittain, S., Evans, A.G., Hutchinson, J.W., Whitesides, G.M., 1998. Spontaneous formation of ordered structures in thin films of metals supported on an elastomeric polymer. Nature 393, 146–149.

Bowden, N., Huck, W.T.S., Paul, K.E., Whitesides, G.M., 1999. The controlled formation of ordered, sinusoidal structures by plasma oxidation of an elastomeric polymer. Applied Physics Letters 75, 2557–2559.

Chen, X., Hutchinson, J.W., 2004. Herringbone buckling patterns of compressed thin films on compliant substrates. Journal of Applied Mechanics-Transactions of the Asme 71, 597–603.

Choi, K.M., Rogers, J.A., 2003. A photocurable poly(dimethylsiloxane) chemistry designed for soft lithographic molding and printing in the nanometer regime. Journal of the American Chemical Society 125, 4060–4061.

Choi, M.K., Song, J., Khang, D.-K., Jiang, H., Huang, Y., Rogers, J.A., 2007. Biaxially stretchable "wavy" silicon nanomembranes. Nano Letters 7, 1655–1663.

Efimenko, K., Rackaitis, M., Manias, E., Vaziri, A., Mahadevan, L., Genzer, J., 2005. Nested self-similar wrinkling patterns in skins. Nature Materials 4, 293–297.

Fu, Y.Q., Sanjabi, S., Barber, Z.H., Clyne, T.W., Huang, W.M., Cai, M., Luo, J.K., Flewitt, A.J., Milne, W.I., 2006. Evolution of surface morphology in TiNiCu shape memory thin films. Applied Physics Letters 89, 3.

Harris, A.K., Wild, P., Stopak, D., 1980. Silicone–rubber substrata – new wrinkle in the study of cell locomotion. Science 208, 177–179.

Harrison, C., Stafford, C.M., Zhang, W.H., Karim, A., 2004. Sinusoidal phase grating created by a tunably buckled surface. Applied Physics Letters 85, 4016–4018.

Huang, Z.Y., Hong, W., Suo, Z., 2005. Nonlinear analyses of wrinkles in a film bonded to a compliant substrate. Journal of the Mechanics and Physics of Solids 53, 2101–2118.

Huck, W.T.S., Bowden, N., Onck, P., Pardoen, T., Hutchinson, J.W., Whitesides, G.M., 2000. Ordering of spontaneously formed buckles on planar surfaces. Langmuir 16, 3497–3501.

Jiang, H., Khang, D.-Y., Song, J., Sun, Y.G., Huang, Y., Rogers, J.A., 2007a. Finite deformation mechanics in buckled thin films on compliant supports. Proceedings of the National Academy of Sciences of the United States of America 104, 15607–15612.

Jiang, H., Sun, Y., Rogers, J.A., Huang, Y.Y., 2007b. Mechanics of precisely controlled thin film buckling on elastomeric substrate. Applied Physics Letters 90, 133119.

Khang, D.Y., Jiang, H.Q., Huang, Y., Rogers, J.A., 2006. A stretchable form of single-crystal silicon for high-performance electronics on rubber substrates. Science 311, 208–212.

Lacour, S.P., Jones, J., Suo, Z., Wagner, S., 2004. Design and performance of thin metal film interconnects for skin-like electronic circuits. IEEE Electron Device Letters 25, 179–181.

Lacour, S.P., Jones, J., Wagner, S., Li, T., Suo, Z.G., 2005. Stretchable interconnects for elastic electronic surfaces. Proceedings of the IEEE 93, 1459–1467.

Lacour, S.P., Wagner, S., Huang, Z.Y., Suo, Z., 2003. Stretchable gold conductors on elastomeric substrates. Applied Physics Letters 82, 2404–2406.

Lacour, S.P., Wagner, S., Narayan, R.J., Li, T., Suo, Z.G., 2006. Stiff subcircuit islands of diamondlike carbon for stretchable electronics. Journal of Applied Physics 100, 6.

Schmid, H., Wolf, H., Allenspach, R., Riel, H., Karg, S., Michel, B., Delamarche, E., 2003. Preparation of metallic films on elastomeric stamps and their application for contact processing and contact printing. Advanced Functional Materials 13, 145–153.

Sharp, J.S., Jones, R.A.L., 2002. Micro-buckling as a route towards surface Patterning. Advanced Materials 14, 799–802.

Stafford, C.M., Guo, S., Harrison, C., Chiang, M.Y.M., 2005. Combinatorial and high-throughput measurements of the modulus of thin polymer films. Review of Scientific Instruments 76, 5.

Stafford, C.M., Harrison, C., Beers, K.L., Karim, A., Amis, E.J., Vanlandingham, M.R., Kim, H.C., Volksen, W., Miller, R.D., Simonyi, E.E., 2004. A buckling-based metrology for measuring the elastic moduli of polymeric thin films. Nature Materials 3, 545–550.

Stafford, C.M., Vogt, B.D., Harrison, C., Julthongpiput, D., Huang, R., 2006. Elastic moduli of ultrathin amorphous polymer films. Macromolecules 39, 5095–5099.

Sun, Y., Choi, W.M., Jiang, H., Huang, Y.Y., Rogers, J.A., 2006. Controlled buckling of semiconductor nanoribbons for stretchable electronics. Nature Nanotechnology 1, 201–207.

Teixeira, A.I., Abrams, G.A., Bertics, P.J., Murphy, C.J., Nealey, P.F., 2003. Epithelial contact guidance on well-defined micro- and nanostructured substrates. Journal of Cell Science 116, 1881–1892.

Timoshenko, S., Gere, J., 1961. Theory of Elastic Stability. McGraw-Hill, New York.

Wagner, S., Lacour, S.P., Jones, J., Hsu, P.H.I., Sturm, J.C., Li, T., Suo, Z.G., 2004. Electronic skin: architecture and components. Physica E-Low-Dimensional Systems & Nanostructures 25, 326–334.

Wilder, E.A., Guo, S., Lin-Gibson, S., Fasolka, M.J., Stafford, C.M., 2006. Measuring the modulus of soft polymer networks via a buckling-based metrology. Macromolecules 39, 4138–4143.

Yoo, P.J., Suh, K.Y., Park, S.Y., Lee, H.H., 2002. Physical self-assembly of microstructures by anisotropic buckling. Advanced Materials 14, 1383–1387.